# MDH2 produced OAA is a metabolic switch rewiring the fuelling of respiratory chain and TCA cycle

Thibaut Molinié, Elodie Cougouilles, C. David, Edern Cahoreau, Jean-Charles Portais, Arnaud Mourier

▶ **To cite this version:**

Thibaut Molinié, Elodie Cougouilles, C. David, Edern Cahoreau, Jean-Charles Portais, et al.. MDH2 produced OAA is a metabolic switch rewiring the fuelling of respiratory chain and TCA cycle. Biochimica biophysica acta (BBA) - Bioenergetics, 2022, 1863 (3), 10.1016/j.bbabio.2022.148532 . hal-03612670

**HAL Id: hal-03612670**
**https://hal.inrae.fr/hal-03612670v1**

Submitted on 18 Mar 2022

**HAL** is a multi-disciplinary open access archive for the deposit and dissemination of scientific research documents, whether they are published or not. The documents may come from teaching and research institutions in France or abroad, or from public or private research centers.

L'archive ouverte pluridisciplinaire **HAL**, est destinée au dépôt et à la diffusion de documents scientifiques de niveau recherche, publiés ou non, émanant des établissements d'enseignement et de recherche français ou étrangers, des laboratoires publics ou privés.

Distributed under a Creative Commons Attribution - NonCommercial - NoDerivatives 4.0 International License

BBA - Bioenergetics 1863 (2022) 148532

Contents lists available at ScienceDirect

BBA - Bioenergetics

journal homepage: www.elsevier.com/locate/bbabio

# MDH2 produced OAA is a metabolic switch rewiring the fuelling of respiratory chain and TCA cycle

Thibaut Molinié [a], Elodie Cougouilles [a], Claudine David [a], Edern Cahoreau [b,c], Jean-Charles Portais [b,c,d], Arnaud Mourier [a,*]

[a] Univ. Bordeaux, CNRS, IBGC, UMR 5095, F-33000 Bordeaux, France
[b] TBI, Université de Toulouse, CNRS, INRA, INSA, Toulouse, France
[c] MetaToul-MetaboHUB, National infrastructure of metabolomics and fluxomics, Toulouse, France
[d] RESTORE, INSERM U1031, CNRS 5070, UPS, EFS, Toulouse, France

ARTICLE INFO

*Keywords:*
Mitochondria
Bioenergetics
MDH2
Oxaloacetate
Malate aspartate shuttle
NADH redox homeostasis
Respiratory chain supercomplexes
Respirasomes

ABSTRACT

The mitochondrial respiratory chain (RC) enables many metabolic processes by regenerating both mitochondrial and cytosolic $NAD^+$ and ATP. The oxidation by the RC of the NADH metabolically produced in the cytosol involves redox shuttles as the malate-aspartate shuttle (MAS) and is of paramount importance for cell fate. However, the specific metabolic regulations allowing mitochondrial respiration to prioritize NADH oxidation in response to high NADH/$NAD^+$ redox stress have not been elucidated. The recent discovery that complex I (NADH dehydrogenase), and not complex II (Succinate dehydrogenase), can assemble with other respiratory chain complexes to form functional entities called respirasomes, led to the assumption that this supramolecular organization would favour NADH oxidation. Unexpectedly, characterization of heart and liver mitochondria demonstrates that the RC systematically favours electrons provided by the 'respirasome free' complex II. Our results demonstrate that the preferential succinate driven respiration is tightly controlled by OAA levels, and that OAA feedback inhibition of complex II rewires RC fuelling increasing NADH oxidation capacity. This new regulatory mechanism synergistically increases RC's NADH oxidative capacity and rewires MDH2 driven anaplerosis of the TCA, preventing malate production from succinate to favour oxidation of cytosolic malate. This regulatory mechanism synergistically adjusts RC and TCA fuelling in response to extramitochondrial malate produced by the MAS.

## 1. Introduction

Mitochondria are organelles present in almost all eukaryotic cells and are essential for the maintenance of cellular metabolism. The oxidative phosphorylation system (OXPHOS) located in the inner mitochondrial membrane (IMM), couples respiration to ATP synthesis [1]. Beyond ATP synthesis, mitochondrial maintenance of NADH/$NAD^+$ redox cofactor balance is of paramount importance for numerous mitochondrial and cytosolic metabolic pathways [2–4]. Redox shuttles, such as the Malate Aspartate Shuttle (MAS), or the α-glycerophosphate shuttle allow mitochondrial respiratory chain (RC) to indirectly oxidize the cytosolic NADH produced by glycolysis and other metabolic pathways [5–7]. The MAS has been demonstrated to be the predominant NADH redox shuttle in highly oxidative tissues as brain, heart and liver [8,9]. This key redox shuttle involves mitochondrial carriers as well as cytosolic and mitochondrial malate dehydrogenases (MDH1, MDH2) and glutamate aspartate transaminases (GOT1, GOT2) [3]. Inter-compartment metabolite cycling through the MAS allows MDH1 and MDH2 to work in opposite directions (oxidizing cytosolic NADH and reducing mitochondrial $NAD^+$) enabling complex I to indirectly oxidize cytosolic NADH. Beyond NADH redox maintenance through Complex I, the RC is also key to sustain the tri-carboxylic acid cycle (TCA cycle) via complex II. This enzyme has recently emerged as focal point of investigation in neurodegeneration [10,11], cardiovascular disorders [12–14], immunology [15], cancer biology [16–18] and signalling [19–21].

The fact that both complex I and II rely on coenzyme Q (CoQ) as common substrate, prompted scientists to investigate molecular

* Corresponding author at: Institut de Biochimie et de Génétique Cellulaires, CNRS-UMR5095, 1, rue Camille Saint-Saëns, CS 61390, 33077 Bordeaux cedex, France.
*E-mail address:* arnaud.mourier@ibgc.cnrs.fr (A. Mourier).

https://doi.org/10.1016/j.bbabio.2022.148532
Received 14 October 2021; Received in revised form 6 January 2022; Accepted 12 January 2022
Available online 19 January 2022
0005-2728/© 2022 The Authors. Published by Elsevier B.V. This is an open access article under the CC BY-NC-ND license (http://creativecommons.org/licenses/by-nc-nd/4.0/).

processes allowing the RC to orchestrate the activity of these two CoQ-oxidoreductases. A recent burst of interest in understanding regulation and activity of CoQ oxidoreductases was triggered by evidence that in contrast to Complex II, the vast majority of Complex I physically interact with other RC complexes III and IV [22]. One of the most important argument for a higher order organization of the RC was provided by the use of blue native polyacrylamide gel electrophoresis (BN-PAGE), which showed that respiratory chain complexes from a wide range of organisms can be extracted in supramolecular assemblies when mitochondria are solubilized using mild detergents [22]. In mammalian mitochondria, supercomplexes (SCs) consisting of complexes I, III, and IV are functional entities consuming oxygen in presence of NADH and are therefore named respirasome [22–24]. Recent studies using a multitude of independent approaches [25–29], have convincingly proven the existence of respirasomes in various organisms. Respirasomes have been reported to play a critical role in bioenergetics and proposed to sequester dedicated pools of CoQ and Cyt *c* in order to function as independent bioenergetic units. It has also been proposed that respirasome could reduce the diffusion distance of CoQ and Cyt *c*, thereby increasing the electron transfer efficiency between complexes organized in respirasomes [30–32]. However, analyses of supercomplex structures, as well as of kinetic and spectroscopic data, do not support substrate channeling by sequestration of CoQ and Cyt *c* [33–35]. Therefore, the bioenergetic roles of respirasomes on mitochondrial NADH oxidation efficiency and on prioritizing electron delivered by complex I against the respirasome-free complex II remain in question.

A growing body of evidence suggests that intramitochondrial oxaloacetate (OAA), identified decades ago as a potent complex II inhibitor [36–39], could play a key role in orchestrating the fuelling of the RC from complex I or II. However, whether or not OAA inhibition of complex II is a metabolically and physiologically relevant process remains controversial. The lack of progress on this essential question most probably lies in the numerous technical constraints, precluding the proper characterization of the OAA metabolic and compartmentation complexity, as well as its chemical instability preventing its quantification by mass spectrometry. Interestingly, recent reports from the Sivitz laboratory characterized mitochondria isolated from different mouse tissues and demonstrated that OAA inhibition of complex II was strongly controlled by mitochondrial membrane potential [40,41].

In this study, we carefully characterize the bioenergetic properties of murine heart and liver mitochondria, as their metabolism strongly depend on MAS [9,42], but also differ in their respective capacity to oxidize NADH versus succinate [43]. Using metabolically active mitochondria, we developed independent biochemical approaches to decipher the respective role of RC supramolecular organization as well as OAA driven complex II inhibition in orchestrating the electron fuelling of the RC from complex I and II. Our results demonstrate that despite the kinetic advantage potentially conferred to NADH oxidation by the assembly of complex I into respirasomes, liver and heart RC prioritize electron provided by complex II. Interestingly, our analyses enlighten the crucial role played by MDH2 in orchestrating electron fuelling of the RC. On one hand, MDH2 mediated OAA production is indispensable to allow mitochondria to metabolize pyruvate and glutamate and to feed complex I with NADH, whereas on the other hand, OAA produced by MDH2 inhibits complex II. Remarkably, the MDH2 rewiring of the RC electrons flow from succinate toward NADH oxidation is triggered by extramitochondrial L-malate at physiological concentration. Consequently, oxidation of imported L-malate by MDH2 does not only rewire the fuelling of the RC from Complex II toward complex I, but concomitantly rewires anaplerosis of TCA cycle, downregulating malate produced by the fumarase to favour oxidation of imported malate. Consequently, MAS does not just passively balance NADH/$NAD^+$ redox between cytosol and mitochondria. Instead, extramitochondrial L-Malate produced by the MAS in response to NADH redox stress can, once imported inside mitochondria, rewires RC electron flow and TCA cycle anaplerosis to increase mitochondrial NADH oxidation and MAS activity.

## 2. Results

### 2.1. Heart and liver mitochondria strongly differ in their NADH and succinate oxidative capacities

To elucidate how mitochondrial RC orchestrates NADH and succinate oxidation we characterized heart and liver mitochondria presenting high TCA and MAS metabolic activities. Bioenergetic characterization of isolated mitochondria was first performed by measuring the oxygen consumption under phosphorylating, non-phosphorylating and uncoupled conditions using high-resolution O2K oxygraphs. To determine the capacity of heart and liver mitochondria to oxidize NADH or succinate, metabolically active mitochondria were incubated in the presence of various nutrient combinations whose metabolism results in delivery of electrons at the level of complex I or complex II. In both heart and liver, we found that simultaneous addition of pyruvate, glutamate and malate was the best combination of nutrient to feed complex I with electrons (Fig. S1A-B). Then, we confirmed that adding complex I inhibitor (rotenone) in presence of succinate was essential to assess maximal complex II driven respiration (Fig. S1C—D). In line with previous observations [43], respirations assessed under phosphorylating or uncoupled conditions were five to three times higher in heart than in liver mitochondria (Fig. 1A-B). Furthermore, our analyses showed that, compared to the succinate driven respiration, heart mitochondria present higher complex I driven respiration (Fig. 1A) than liver mitochondria (Fig. 1B). This observation prompted us to decipher if the difference in complex I and II driven respirations, was caused by mitochondrial metabolic constraint affecting NADH or succinate provisional of the RC or to intrinsic RC functional discrepancies. To bypass potential thermodynamic and kinetic controls linked to metabolite transport or internal metabolism, we permeabilized mitochondria to specifically measure RC activity fed directly with NADH or succinate. To evaluate how mitochondrial permeabilization impacts RC activity, we have compared different permeabilization methods (freeze/thaw cycles, Alamethycin or digitonin) and we observed no gross difference between complex I and II driven respirations measured. Interestingly, when RC is directly fuelled with reduced substrates, heart RC can oxidize NADH two time faster than succinate (Fig. 1C) whereas an opposite situation is observed in liver RC (Fig. 1D). The high disparity in NADH and succinate oxidation rates observed between heart and liver RC prompted us to further characterize tissue specific RC composition changes. To this end, we quantified RC complex levels assessing cytochromes (Fig. 1E) and multiple OXPHOS protein levels (Fig. 1F-H). These two independent approaches consistently showed that all cytochromes as well as RC complex subunits were two to four times more abundant in heart than in liver mitochondria (Fig. 1E-G). Moreover, the relative abundance of complex I normalized to complex II was almost tripled in heart compared to liver (Fig. 1H). Altogether, the data presented in Fig. 1 show that RC complexes content and stoichiometry strongly differ between heart and liver (Fig. 1E-H) and that these differences correlate with tissue specific functional differentiation (Fig. 1A-D). Interestingly, when both complex I and complex II substrates are added to mitochondria, the increase in RC activity is too low to sustain both NADH and succinate oxidation flow at maximal speed (Fig. 1A-D). This observation prompted us to develop assays allowing to determine the respective contribution of complex I and complex II in feeding RC with electrons, when both NADH and succinate are present.

### 2.2. Heart and liver respiratory chain preferentially oxidize succinate over NADH

The respective contribution of NADH and succinate oxidation in fuelling RC with electrons when mitochondria are in presence of both substrates, was first evaluated using permeabilized mitochondria. This

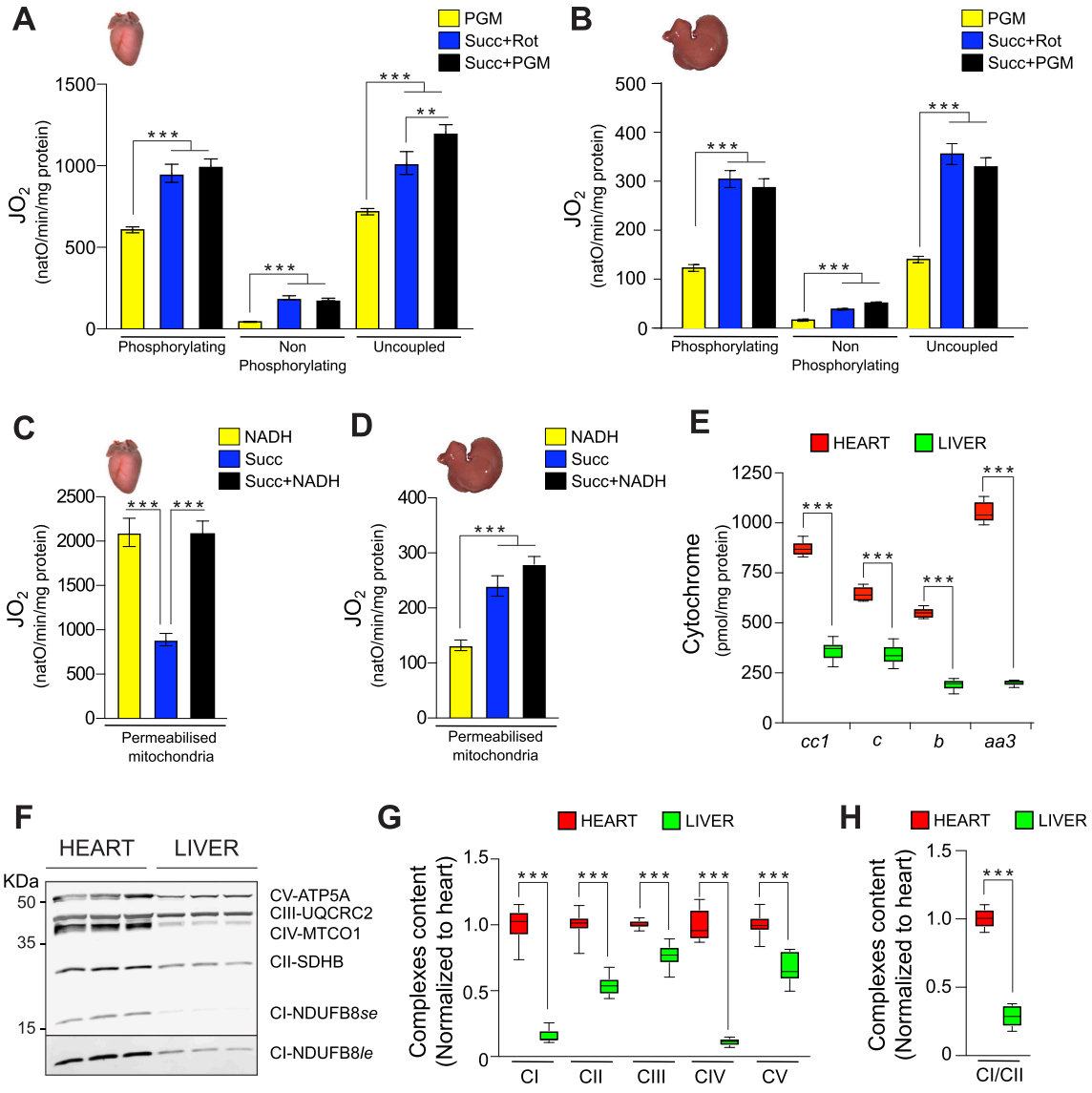


**Fig. 1.** Heart and liver respiratory chain composition and bioenergetics.
(A, B) Oxygen consumption of intact heart (A) and liver (B) mitochondria assessed in presence of mitochondrial complex I substrates (PGM: pyruvate 10 mM, glutamate 5 mM, malate 5 mM), or complex II substrate (Succ+Rot: Succinate 10 mM and rotenone 30 nM), and PGM and succinate (Succ+PGM). Respiration are assessed under phosphorylating conditions (ADP + Pi), non-phosphorylating conditions (oligomycin), and uncoupled (CCCP titration). Heart ($n = 15$), liver ($n = 5$), error bars represent the mean ± SEM.
(C, D) Oxygen consumption of permeabilised heart (C) and liver (D) mitochondria assessed in presence of NADH (1.2 mM), Succinate (10 mM) and cytochrome *c* (62.5 µg/ml). Heart ($n = 10$), liver ($n = 12$), Error bars represent the mean ± SEM
(E) Mitochondrial cytochrome quantified from redox absorbance spectra. Cytochromes content of RC complexes: complex III (*b*, *c1*), complex IV (*aa3*) and cytochrome *c* (*c*) were determined in mitochondrial extracts of heart and liver. Heart ($n = 6$) liver (n = 6), error bars represent the mean ± SEM.
(F) Steady-state levels of OXPHOS subunits, in heart and liver mitochondria, determined by western blot analyses. Short and long exposure are performed to detect complex I (complex I *se* and complex I *le*) in the liver. Representative Western-blot of five different experiments.
(G) Relative amount of OXPHOS complexes (complex I– complex V) in heart and liver mitochondria determine by densitometric quantification of western blot experiments presented in (F), and normalized to heart OXPHOS complexes. (n = 5) Error bars represent the mean ± SEM
(H) Relative amount of complex I normalized to complex II in heart and liver mitochondria determined by densitometric analyses, (n = 5) Error bars represent the mean ± SEM.

system is particularly well suited to determine the sources of electrons feeding the respiratory chain as it allows (i) to provide non-limited amount of NADH and succinate and follow their oxidation rate, (ii) to remove thermodynamic constraints linked to the protonmotive force on complex I and on the RC activity, (iii) to bypass kinetic controls due to metabolites import and internal metabolism and prevent also metabolic reduction of $NAD^+$ generated by complex I. First, the respective contribution of NADH and succinate in fuelling the RC was assessed using validated and highly specific complex I or II inhibitors i.e. rotenone (Rot) and Atpenin A5 (AtpnA5) (Fig. S2A-D). As presented in Fig. 1 C and D, mitochondrial respiration of permeabilized mitochondria assessed in presence of both NADH and succinate is not sufficient to sustain both NADH and succinate oxidation flux at their maximal capacity (respiration assessed with NADH or succinate added alone). Surprisingly our analyses demonstrate that limiting RC capacity is not evenly affecting NADH and succinate oxidation fluxes when heart and liver RC are simultaneously fed with both NADH and succinate (Fig. 2A-D). Instead, our results show that when permeabilized heart and liver

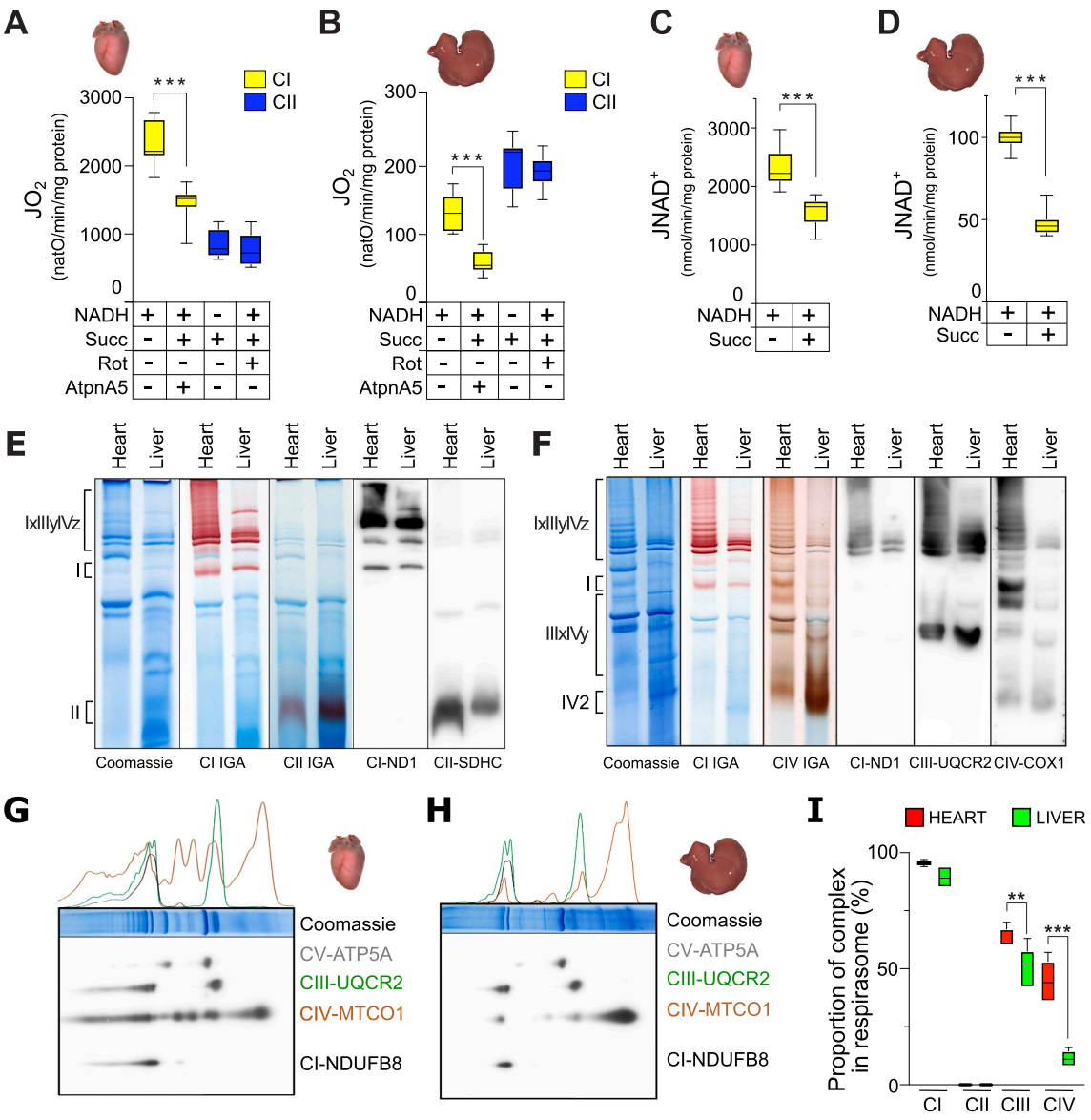


**Fig. 2.** Heart and liver respiratory chain supramolecular organization and preferential electron fuelling.

(A, B) Oxygen consumption of permeabilised mitochondria isolated from heart (A) and liver (B) assessed in presence of cytochrome *c* (62.5 μg/ml), complex I substrate NADH (1.2 mM), complex II substrate succinate (Succ, 10 mM) or both substrates simultaneously added. Addition of complex I (rotenone, 30 nM) or complex II (atpeninA5, 20 nM) specific inhibitor is used to discriminate complex I driven respiration (yellow) and complex II driven respiration (blue) when mitochondria are incubated with NADH and succinate. Heart ($n$ = 9), Liver (n = 12), error bars represent the mean ± SEM

(C, D) complex I driven $NAD^+$ synthesis flux assessed in permeabilised mitochondria isolated from heart (C) and liver (D), incubated in presence of cytochrome *c* (62.5 μg/ml), complex I substrate NADH (1.2 mM) and/or complex II substrate succinate (Succ, 10 mM). Heart ($n$ = 6), liver (n = 9), error bars represent the mean ± SEM.

(E, F) Supramolecular organization of heart and liver RC. Heart and liver mitochondria are solubilized with a digitonin/protein ratio of 3:1 (g/g) and RC are resolved with 4–16% (E) or 3–12% (F) BN-PAGE, followed by complex I-, complex II- and complex IV-IGA assays, or by western blot using antibody toward ND1, SDHC, UQCRC2 or COX1 subunits. Representative of three different experiments. Heart ($n$ = 3), liver (n = 3).

(G, H) RC complexes composition of heart (G) and liver (H). Supramolecular organization of RC is assessed by 2D-BN/SDS-PAGE and immunoblot analyses are performed with OXPHOS cocktail antibodies toward NDUFB8, MTCO1, UQCR2 and ATP5A subunits. Densitometric profile of complex I (black), complex III (green) and complex IV (orange) detected by immunoblot are represented on top of Coomassie staining. Representative of three different experiments. Heart (n = 3), liver (n = 3).

(I) Relative amount of complex I, complex II, complex III and complex IV associated in respirasome (complex I-III-IV) or in supercomplexes containing complex I (complex $I_x$-$III_y$ or complex $I_x$-$IV_y$) in heart (red bars) and liver (green bars). Proportion of complexes found associated in respirasome is determined by densitometric quantification of 2D-BN/SDS-PAGE. Heart (n = 3), Liver (n = 3), Error bars represent the mean ± SEM. (For interpretation of the references to colour in this figure legend, the reader is referred to the web version of this article.)

mitochondria are incubated with both NADH and succinate, complex II driven respiration was not significantly affected compared to the maximal succinate driven respiration assessed when succinate is the unique electron source fuelling the RC (Fig. 2A-B). In contrast, the NADH driven respiration was strongly decreased in presence of succinate compared to the maximal NADH driven respiration determined when NADH is the unique electron source fuelling the RC (Fig. 2A-B). This significant decrease of the complex I driven respiration in presence

of succinate, was confirmed by enzymatic measurement of the $NAD^+$ production rate (Fig. 2C-D). Interestingly, despite the great disparity in their respective complex I and II contents and oxidative capacities (Fig. 1C-D), the priority given to complex II electrons in presence of both NADH and succinate, was consistently observed in both heart and liver mitochondria (Fig. 2A-D).

The finding that liver and heart RC preferentially oxidize succinate over NADH was in stark contrast to recent hypothesis supporting the fact that the structural association of complex I with complex III and IV should confer kinetics advantage to NADH oxidation over electrons provided by the respirasome free complex II [32,44]. This surprising result prompted us to investigate the supramolecular organization of heart and liver RC. To this end, mitochondria were solubilized using digitonin (at a ratio of 3 g digitonin per g protein) and the supramolecular organization of the RC was then resolved using standard BN-PAGE technique and analyzed by western blotting or in-gel activity assay (IGA) (Figs. 2E-F and S2E-G). First, BN-PAGE profiles presented in the Fig. 2E and F clearly confirmed the striking enrichment of heart RC in complex I and IV compared to liver RC, supporting our previous observations (Fig. 1E-G). Interestingly, these changes in RC complexes stoichiometry between the two tissues remarkably correlate with the abundance and diversity of respirasomes (IxIIIyIVz) (Fig. 2E-F). To determine the proportion of complex I and II assembled in supercomplexes, BN-PAGE first dimension was further resolved in a second denaturing dimension. 2D-SDS-PAGE is commonly used to properly quantify the protein levels as they prevent potential epitope accessibility issues encountered with native proteins. Remarkably, 2D electrophoresis analyses were in agreement with previous studies [45,46] showing that more than 90% of heart and liver complex I are found associated in respirasomes whereas no detectable complex II could be found associated in supercomplexes (Figs. 2E-I and S2E-G). Furthermore, the supramolecular organization of complex I and II with other RC is not plastic as no significant respirasome reshuffling could be observed when BN-PAGE experiments were performed solubilizing mitochondria

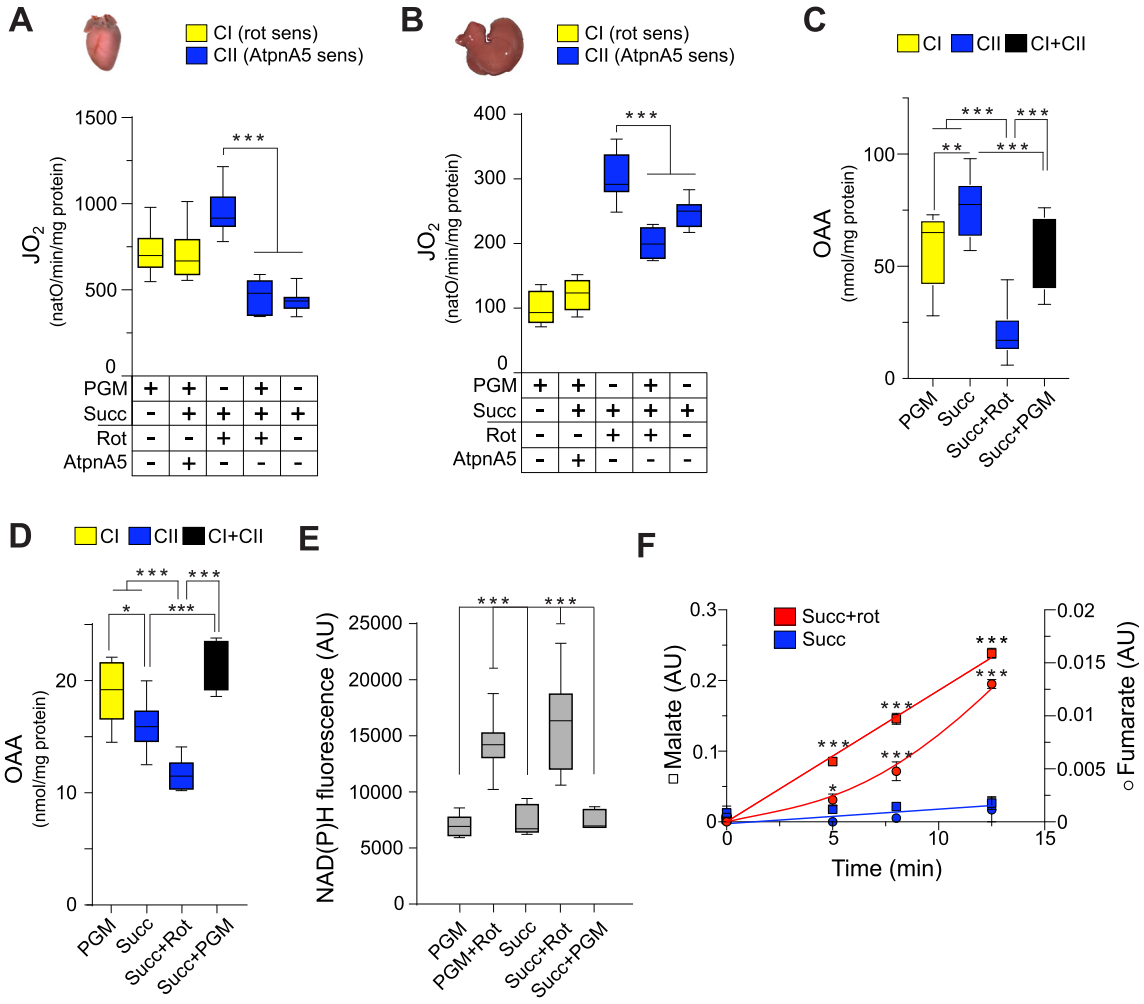


**Fig. 3.** Internal OAA level orchestrates the respective contribution of complex I and II to feed the respiratory chain with electrons

(A, B) Oxygen consumption of uncoupled heart (A) and liver (B) intact mitochondria assessed in presence of complex I substrates (PGM) and/or complex II substrate (Succ). Addition of complex I (rotenone, 30 nM) or complex II (atpeninA5, 20 nM) specific inhibitor is used to discriminate complex I dependent respiration (yellow bars) and complex II dependent respiration (blue bars) when mitochondria are incubated with PGM and Succ. Heart ($n = 17$), liver (n = 6), error bars represent the mean ± SEM.

(C, D) Oxaloacetate levels assessed when uncoupled heart (C) and liver (D) intact mitochondria are fed with complex I substrates (PGM) and/or complex II substrate (Succ). Heart ($n = 4$), Liver (n = 3), Error bars represent the mean ± SEM.

(E) Mitochondrial NAD(*P*)H fluorescence of uncoupled heart mitochondria incubated with complex I substrates (PGM) ± rotenone (30 nM), or complex II substrate (Succ) ± rotenone (30 nM), or both (Succ+PGM). ($n = 5$), error bars represent the mean ± SEM.

(F) 1H—1D NMR quantification of fumarate (circle) and malate (scare) content are assessed in uncoupled heart mitochondria oxidizing succinate in absence (blue) or in presence of rotenone (30 nM) (red). (n = 3), error bars represent the mean ± SEM. (For interpretation of the references to colour in this figure legend, the reader is referred to the web version of this article.)

actively metabolizing different respiratory substrates (Fig. S2H-I). Altogether, our results indicate that despite the absence of stable physical interaction between complex II and other RC complexes, succinate oxidation is prioritized over electrons delivered by complex I. However, to challenge the physiological relevance of the preferential succinate oxidation observed with permeabilized mitochondria, we sought to investigate NADH and succinate fuelling of the RC in metabolically active mitochondria.

### 2.3. Internal oxaloacetate level orchestrates the respective contribution of complex I and II to respiration

To evaluate potential metabolic outcomes of the preferential succinate oxidation on TCA and MAS cycle activities, we applied our new experimental strategy deciphering the origin of electrons fuelling the RC on intact and metabolically active mitochondria. In intact mitochondria, succinate is transported through dicarboxylate carrier before being directly oxidized by complex II. In contrast, NADH cannot be directly imported and will have to be metabolically generated from matrix dehydrogenases like malate, glutamate or pyruvate dehydrogenases. Use of specific inhibitor demonstrated that mitochondrial respiration assessed in presence of pyruvate, glutamate, and malate (PGM) totally relied on complex I activity as this respiration was abolished by rotenone (Fig. S2A and C). Similarly, succinate driven respiration was inhibited in presence of AtpeninA5 (Fig. S2B and D). Interestingly, uncoupled respiration assessed in presence of succinate and rotenone (Fig. 3A-B) was almost identical to succinate driven respiration measured on permeabilized mitochondria (Fig. 2A-B). However, when succinate driven uncoupled respiration was assessed in absence of rotenone, respiration values were decreased by 40% in heart and 30% in liver mitochondria (Figs. 3A-B and S1C-D). The necessity to add rotenone to assess maximal succinate driven respiration on metabolically active mitochondria has been explained as complex I inhibition could prevent accumulation of oxaloacetate (OAA) a potent competitive inhibitor of complex II [37,40,47]. To characterize the specificity and the metabolic relevance of OAA inhibition, permeabilized mitochondria incubated with succinate or NADH were recorded in presence of increasing concentration of OAA (Fig. S3A). These analyses clearly demonstrated that OAA is a powerful and highly specific complex II inhibitor, as no inhibitory side effects could be observed on NADH driven respiration. To elucidate the potential regulatory function of OAA on succinate respiration in intact mitochondria, we developed an enzymatic assay to quantify OAA levels (Fig. 3C-D). Our analyses performed on both heart and liver mitochondria confirmed that the stimulation of succinate respiration by rotenone (Fig. 3A and B) was associated with a striking lowering of OAA level (Fig. 3C-D). As expected, extemporaneous fluorometric measurement of mitochondrial internal NAD(*P*)H level demonstrated that inhibition of complex I by rotenone massively increased mitochondrial redox (NAD(*P*)H) state (Figs. 3E and S3B). Interestingly, NMR spectroscopy analyses showed that treatment of succinate-metabolizing mitochondria with rotenone, provoked an excretion of malate and fumarate (Fig. 3F). Altogether, our analyses support that the increase in NADH/$NAD^+$ ratio secondary to complex I inhibition by rotenone could prevent MDH2 driven OAA accumulation (Fig. 3C-D) which consequently increases succinate respiration (Fig. 3A-B).

To determine the respective contribution of complex I and II in fuelling RC with electrons on intact mitochondria, we applied the inhibitor-driven approach. This approach was validated on intact mitochondria as rotenone and atpeninA5 sensitive respirations, assessed under uncoupled conditions, were additive and independent of the sequence of addition of inhibitors (Fig. S3C-D). Intriguingly, in contrast to the results obtained on permeabilized mitochondria (Fig. 2A-B), complex I dependent respiration was preserved in presence of multiple substrates, whereas complex II respiration was similar or even lower than the 'OAA inhibited' succinate respiration measured in absence of rotenone (Fig. 3A-B). Interestingly, the OAA levels perfectly matched the degree of inhibition of the succinate respiration when all substrates were provided to heart (Fig. 3C) and liver (Fig. 3D) mitochondria. Altogether, our data identified OAA as a key metabolic regulator orchestrating the respective contribution of complex I and II to RC electron flow. The OAA regulation occurring in intact mitochondria could totally counteract the natural RC priority given to complex II, to favour NADH oxidation.

### 2.4. MDH2 is a metabolic switch rewiring respiratory chain and TCA fuelling

The importance of MDH2-generated OAA in orchestrating mitochondrial NADH or succinate oxidation, prompted us to investigate the metabolic relevance of this new regulatory mechanism. MDH2 is a mitochondrial metabolic checkpoint located at the crossroad of TCA cycle and MAS (Fig. 4A). To decipher the functional interplay between MAS, RC and TCA cycle, we assessed complex II driven respiration mimicking a cytosolic NADH redox stress by increasing the extramitochondrial malate level within physiologically relevant concentration range (Fig. 4A) [7,48,49].

This experiment demonstrated that complex II driven respiration decreased proportionally in response to increased malate concentration (Figs. 4B-D and S4A-C). As control, we showed that malate per se did not impact succinate respiration in permeabilized mitochondria (Fig. S4D). This observation further explained why malate inhibition only occurred in metabolically active mitochondria where OAA can be generated and accumulated. In line with this observation, the decrease in complex II driven respiration associated with increase malate concentration was perfectly correlated with an increase in mitochondrial OAA level (Figs. 4D and S4C). Altogether, our data show that more than 60% of complex II driven respiration can be downregulated in response to increased extramitochondrial malate concentration through a MDH2-mediated metabolic regulation in both heart and liver.

To confirm that OAA could act as mitochondrial metabolic sensor adjusting RC fuelling to mitochondrial metabolic activity, we investigated how mitochondrial metabolic pathways consuming OAA could impact succinate and NADH dependent respirations. To this end, mitochondrial RC activity was assessed in presence of succinate (Succ) and glutamate (Glu) or/and pyruvate (Pyr) to metabolically flush OAA through MAS (GOT2 dependent pathway) or through the TCA cycle (pyruvate dehydrogenase and citrate synthase dependent pathway) (Fig. 4A). Our analyses demonstrated that both pyruvate and glutamate were efficient in consuming internal OAA as both substrates added alone or in combination decreased OAA to similar residual level as the one measured in presence of succinate and rotenone (Figs. 4E and S4E). The metabolic flush of OAA did not only increase succinate driven respiration by releasing complex II inhibition, but it also fuelled complex I with NADH (Figs. 4F and S4F). Eventually, we decided to determine if MDH2 could metabolically rewire RC electrons entry from succinate toward NADH, when MAS driven external NADH oxidation demand is increased (increasing malate concentration within physiological range). Our results clearly showed that Malate-OAA dependent respiration rewiring from complex II to complex I occurs, even when OAA produced by the MDH2 is metabolically flushed through MAS and TCA cycle (Fig. 4G). Remarkably, imported malate oxidized through MDH2 not only downregulates succinate driven respiration, but it also increases MDH2 driven NADH production and complex I driven NADH oxidation capacity.

## 3. Discussion

Our present work indicates that the differences between heart and liver mitochondrial bioenergetics activities mainly correlate with change in abundancy and stoichiometry of OXPHOS complexes. For instance, differences in complex I and II levels (Fig. 1H) are in line with the different NADH and succinate driven respiration capacities of heart and liver mitochondria (Fig. 1A-D). In contrast, the proportion of complex I and II assembled into respirasome is not changed between heart

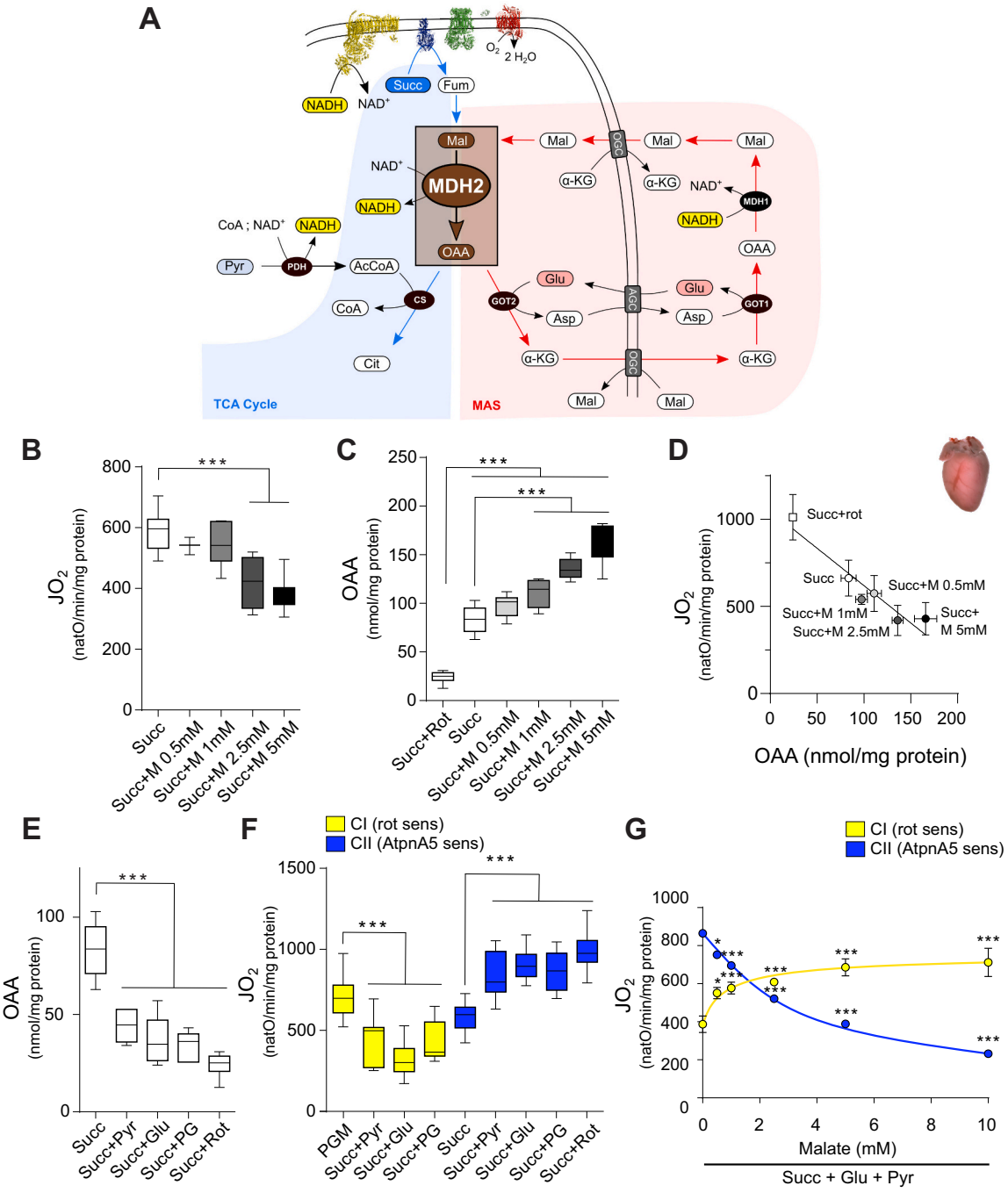


**Fig. 4.** MDH2 produced OAA rewires TCA cycle and respiratory chain electron flows to favour NADH oxidation

Scheme of respiratory chain, TCA cycle (blue background), and malate-aspartate shuttle (MAS, red background) enlightening the key metabolic role played by MDH2. Abbreviations: succinate (Succ), fumarate (Fum), malate (Mal), oxaloacetate (OAA), glutamate (Glu), aspartate (Asp), α -ketoglutarate (α-KG), acetyl-CoA (AcCoA), citrate (Cit), pyruvate (Pyr), aspartate-glutamate carrier (AGC) 2-oxoglutarate carrier (OGC), malate dehydrogenase (MDH1, MDH2), glutamate-oxaloacetate transaminase (GOT1,GOT2), citrate synthase (CS), pyruvate dehydrogenase (PDH)

(B, C) Oxygen consumption (B) and oxaloacetate level (C) assessed with intact heart mitochondria fed with succinate and increased concentration of malate (M) during uncoupled respiration. ($n$ = 4), error bars represent the mean ± SEM.

(D) Correlation between mitochondrial oxygen consumption and oxaloacetate levels of intact heart mitochondria isolated fed with succinate and increased concentration of malate (M). Error bars represent the mean ± SEM.

(E) Oxaloacetate levels assessed with intact heart mitochondria in presence of different substrates condition metabolizing endogenously produced OAA (Succ+Glu, Succ+Pyr, Succ+PG). (n = 4), error bars represent the mean ± SEM.

(F) Oxygen consumption of intact heart mitochondria fed with indicated substrates (Succ+Glu, Succ+Pyr, Succ+PG). Addition of specific inhibitor of complex I (rotenone, 30 nM) and complex II (AtpeninA5, 20 nM) during uncoupled respiration, determine the complex I driven respiration (yellow bars) or complex II driven respiration (blue bars). ($n$ = 8), error bars represent the mean ± SEM.

(G) Correlation between oxygen consumption of intact heart mitochondria fed with succinate, pyruvate, glutamate and increasing concentration of malate. Complex I driven (yellow circle) or complex II driven (blue circle) respiration are determined through sequential addition of specific complex I (rotenone, 30 nM) and complex II (AtpeninA5, 20 nM) inhibitors. (n = 4), error bars represent the mean ± SEM. (For interpretation of the references to colour in this figure legend, the reader is referred to the web version of this article.)

and liver RC (Figs. 2E-I and S2E-I). In line with previous works performed in different tissues or model organisms, the supramolecular organization of mouse heart and liver RC demonstrates that about 90% of complex I is associated in supercomplexes whereas complex II is never found associated with other RC complexes [45,46]. This striking difference in the supramolecular organization of the CoQ-oxidoreductases led to the assumption that the physical association of complex I with other RC complexes could reduce the diffusion distance of CoQ and Cyt c between organized complexes, promoting NADH oxidation [30–32]. To decipher the functional relevance of the supramolecular organization of the complex I and II on their ability to fuel the RC, we developed a new experimental strategy using permeabilized mitochondria to (i) provide non-limited amount of NADH and succinate and follow their oxidation rate, (ii) remove thermodynamic constraints linked to the protonmotive force on complex I and on the RC activity, (iii) prevent the interfering inhibition of complex II by OAA. Surprisingly, the inhibitor driven approach as well as multiple flux ($JNAD^+$ and $JO_2$) analyses consistently demonstrates that when permeabilized mitochondria are incubated with both NADH and succinate, the complex II driven respiration is preserved whereas complex I driven respiration is strongly decreased in heart and liver mitochondria (Fig. 2A-D). Interestingly, the fact that NADH driven respiration is drastically reduced in the presence of succinate clearly demonstrates that the respirasome is not functionally disconnected from the respirasome free complex II (Fig. 2C-D). Our observations indicate that respirasomes structuration does not lead to strict, physical and functional, partitioning between RC complexes and electrons carriers (CoQ and Cyt c) and thus support previous work [31,33,34]. The discovery of a mechanism enabling the RC to orchestrate the activities of coenzymes Q oxidoreductases constitutes a major conceptual breakthrough in the field of mitochondrial energy metabolism. This regulatory mechanism called 'electron competition' or 'CoQ-contest' originally discovered in *S. cerevisiae* allows the yeast RC to prioritize oxidation of cytosolic NADH [50–52]. The fact that, in contrast to succinate oxidation, the NADH driven respiration is found drastically affected when heart and liver RC are incubated with both NADH and succinate clearly demonstrate that the 'CoQ contest' mechanisms is not restricted to the yeast model but also orchestrates mammalian heart and liver RC electron flow (Fig. 2A-D). Moreover, in line with observations made with yeast, the priority given to certain CoQ-oxidoreductase is (i) independent of the RC supramolecular organization [53] and (ii) independent of the stoichiometry between CoQ-oxidoreductases involved (Figs. 1F-H and 2E-F).

The paramount importance of the maintenance of the $NADH/NAD^+$ redox balance by the mitochondria for cell metabolism and cell functions was consistently observed in various eukaryotes models expressing different fermentative pathways and presenting different NADH CoQ-oxidoreductase systems fuelling the RC [54–57]. In humans complex I or redox shuttles loss of functions cause numerous pathologies and the resulting NADH redox imbalance often lead to life-threatening lactic acidosis crises [58–61]. Recent studies have shown that the control of the cellular redox balance by the mitochondria is essential for the maintenance of cellular proliferative capacities [62,63]. Until recently, mitochondria were described as being impermeable to $NAD^+$/NADH [64]. However, this dogma has been recently challenged by the demonstration that NAD(H) could be imported in mammalian mitochondria [65] and by the identification of SL25A51 as a mammalian mitochondrial NAD(H) transporter [66] compensating the absence of intramitochondrial NAD(H) synthesis. However, the rate of NADH import through this transporter is extremely limited and therefore is not directly involved in connecting cytosolic and mitochondrial $NADH/NAD^+$ redox homeostasis. Instead, connection between the cytosolic and mitochondrial redox homeostasis is ensured by redox shuttles such as the MAS [8,9].

The impressive enzymatic equipment metabolizing cytosolic and mitochondrial OAA demonstrates its metabolic importance and positioned this metabolite at the crossroad between glycolysis (Pyruvate Carboxylase 1 and 2), gluconeogenesis (PEPCK1, PEPCK2), TCA cycle (MDH2, CS) and Malate aspartate Shuttle (MDH1, MDH2, GOT1, GOT2). Bioenergetic analyses of heart and liver mitochondria, early on characterized through their high MAS metabolic capacities [9,42], support recent work from the Sivitz group claiming that regulation of complex II activity by OAA is of great metabolic interest [40,41]. Our analyses extend and refine mitochondrial metabolic processes controlling internal OAA levels and therefore regulating the complex II activity. Importantly, our data demonstrate that MDH2 acts as a metabolic conductor synergistically orchestrating RC and TCA activity adjusting mitochondrial NADH oxidation to MAS activity. First, our work confirms that production of OAA by MDH2 relies on mitochondrial redox (NADH/NAD+) maintenance by complex I and can be abolished when complex I is inhibited by rotenone (Figs. 3C-F and S3B). Secondly, the complex II inhibition caused by MDH2 driven OAA production can be completely reversed when OAA is metabolized by PDH and CS (succ+pyr) or GOT2 (succ+glut) (Fig. 4E-F). Surprisingly, we show that extra-mitochondrial malate, added at physiologically relevant concentrations range, can increase internal OAA, leading to a dominant inhibition of complex II, rewiring RC electrons fuelling as well as the TCA anaplerosis. This dose dependent inhibition of the complex II driven respiration by extra-mitochondrial malate is associated with an increase in complex I driven respiration (Fig. 4G). Beyond complex II inhibition, MDH2 activity is crucial to sustain complex I activity through direct NADH production and by producing OAA indispensable for mitochondrial metabolism of pyruvate and glutamate (Fig. S1A-B). Moreover, the immediate and reversible inhibition of complex II by OAA indicate that mitochondrial OAA levels could act as a metabolic sensor adjusting electrons fuelling the RC to fit cell metabolic needs. This metabolic regulation synergistically increases RC's NADH oxidative capacity and rewires MDH2 driven TCA anaplerosis, preventing malate production from succinate to favour oxidation of imported malate (Fig. 4G). This discovery prompts us to hypothesise that MAS does not only passively balance cytosolic and mitochondrial NADH but instead, through MDH2 oxidation of imported malate, MAS actively rewires RC's fuelling, and TCA anaplerosis to boost complex I activity and fuelling.

To conclude, our work first demonstrated that permeabilized heart and liver mitochondria incubated with both NADH and succinate prioritize RC fueling from succinate. This observation challenges recent hypothesis supporting that the supramolecular organization of complex I with other RC complexes could favour RC fueling from NADH against the respirasome free complex II. Furthermore, multilevel analyses performed on permeabilized and metabolically active mitochondria demonstrate that the preferential succinate driven respiration is tightly controlled by intramitochondrial OAA level. Altogether, our analyses demonstrate that the MDH2 produced OAA can synergistically rewire the fuelling of the RC and TCA cycle to adjusts RC's NADH oxidative capacity in response to extramitochondrial malate metabolically produced by the MAS.

## 4. Experimental procedures

### 4.1. Biological materials

All mice used in this study were inbred C57Bl/6N background. The bioenergetic phenotype presented in this manuscript is not gender specific and therefore analyses performed with isolated heart and liver mitochondria isolated from male and female were pooled. Mice were maintained on a standard mouse chow diet and sacrificed, between 20 and 40 weeks of age, by cervical dislocation in strict accordance with the recommendations and guidelines of the Federation of the European Laboratory Animal Science Association, and obtain with an authorization from the French ministry of Agriculture (APAFIS#12648-2017112083056692v7).

### 4.2. Heart and liver mitochondria isolation

Isolation of heart and liver mitochondria was performed by differential centrifugation allowing to obtain a mitochondrial fraction with high purity degree while preserving their metabolic and bioenergetic state. The purity and intactness of this isolation protocol was previously demonstrated through FACS and electron tomography analyses [43,67]. Briefly, right after the sacrifice, tissues were collected, minced and cleaned with mitochondria isolation buffer (MIB; 310 mM sucrose, 20 mM Tris-Base, 1 mM EGTA, pH 7.2) for the heart and MIB + BSA (MIB and 0.25 mg/ml of delipidated Bovine serum albumin (BSA)) for the liver. The pieces of heart were collected and homogenized with few strokes of a Potter S homogenizer (Sartorius) using a loose Teflon pestle, in an ice cold MIB supplemented with trypsine (0.5 g/l). Liver tissues homogenisation was performed in a Potter S homogenizer (Sartorius) using a Teflon pestle, and in ice cold MIB + BSA. Mitochondria were isolated by differential centrifugation, a low speed one (1000 g, 10 min, 4° C) in a swing out rotor and another one at high speed (3500 g, 10 min, 4 °C for heart mitochondria and 10,000 g, 10 min, 4° C for liver mitochondria) using a fixed angle rotor. The pellet of crude mitochondria obtained is suspended in MIB + BSA. Protein concentration was measured using Bio-Rad DC Protein Assay kit according to provider's instructions.

### 4.3. High-resolution oxygen consumption measurement

Oxygen consumption of intact crude mitochondria was measured at 37 °C, using respectively 50 μg and 100 μg of heart and liver mitochondria diluted in 2.1 ml of respiratory buffer (RB: 120 mM sucrose, 50 mM KCl, 20 mM Tris-HCl, 4 mM $KH_2PO_4$, 2 mM $MgCl_2$, 1 mM EGTA, 0.25 mg/ml delipidated BSA; pH 7.2) in an Oxygraph-2 k (OROBOROS INSTRUMENTS, Innsbruck, Austria) [68]. Oxygen consumption was measured by using different association of substrates: succinic acid (10 mM; pH 7.2), sodium pyruvate (10 mM; pH 7.2), L-Glutamate acid (5 mM; pH 7.2), L-Malic acid (concentrations are indicated in the figure legends; pH 7.2). Oxygen consumption rate was measured under 3 different conditions: in the phosphorylating state with addition of ADP (5 mM; pH 7.2), in the non-phosphorylating state with addition of oligomycin (50 ng/ml), and in the uncoupled state by successive addition of carbonyl cyanide *m*-chlorophenyl hydrazone (CCCP) up to 0.5 μM to reach the maximal respiration of the RC.

Activity of the RC was also recorded using permeabilized crude mitochondria obtain after freeze and thaw cycle. Oxygen consumption by the RC was measured as previously described [68], using respectively 50 and 100 μg of heart and liver mitochondria diluted in 2.1 ml of potassium phosphate buffer (50 mM, pH 7.2) and incubated with saturating concentrations of cytochrome *c* (62.5 μg/ml), NADH (0.625 mM) and succinate (10 mM) . No oxygen consumption could be detected in absence of cytochrome *c*, and no oxygen consumption link to complex I activity was recorded when permeabilized mitochondria are incubated with pyruvate, glutamate and malate, confirming the loss of integrity of mitochondrial internal compartment.

The determination of oxygen consumption link to electron coming from complex I and complex II was determined after addition of rotenone (Rot, 30 nM) for complex I and/or atpenin A5 (AtpnA5, 20 nM) for complex II. As a control, Antimycin A (100 nM) was added at the end of each experiment to control the proportion of oxygen consumption which is not linked to RC.

### 4.4. Mitochondrial cytochromes quantification

The different cytochromes of the mitochondrial respiratory chain were measured by dual-wavelength spectrophotometry by comparing the spectra of fully oxidized vs. fully reduced cytochromes. In each of the two cuvettes, 2 mg of heart or 16 mg of liver mitochondrial protein were suspended in 1 ml of phosphate buffer (50 mM, pH 7.2), and 0.05% (vol/vol) Triton X-100 were added. In the "oxidized" cuvette, 10 μl of ferricyanide (0.5 M) were added while a few grains of sodium hydrosulfite were added in the "reduced" cuvette. The components were mixed, and the absorbance spectrums of both cuvettes were recorded. A typical difference between reduced minus oxidized spectra was obtained. Wavelength pairs and absorption coefficient used were: cytochrome *c* + *c1* (550–540 nm) $\varepsilon = 18\ mM^{-1}/cm$, cytochrome *b* (563–575 nm) $\varepsilon = 18\ mM^{-1}/cm$ and cytochrome *a* + *a3* (605–630 nm) $\varepsilon = 24\ mM^{-1}/cm$.

### 4.5. Western-blot analyses

Proteins from crude heart and liver mitochondria were resolved using denaturing (SDS PAGE or native electrophoreses (BN-PAGE and Second dimensional SDS PAGE)).

For SDS PAGE, 50 μg of heart and liver crude mitochondria proteins were solubilized with RIPA buffer (NaCl (150 mM), tris-base (25 mM), NP40 (1% *w/v*), SDS (1% w/v), deoxycholate (0.25% w/v) and EGTA (1 mM), pH 8). Solubilized mitochondria were mixed with Laemmli buffer [69], separated by Bis-Tris 15% acrylamide gel, and then transferred on nitrocellulose Amersham Protran Premium membrane (Amersham). Immunodetection was performed by fluorescence using a Typhoon FLA 9500 (GE Healthcare Life Sciences). To perform immunodetection, membranes were blocked with 3% (*w/v*) milk diluted in Tris Buffer Saline (TBS; pH 8), then primary antibody (Total OXPHOS Rodent WB Antibody Cocktail; ab110413 Abcam) was added for incubation, and finally an ECL Plex™ G-A-R IgG, Cy®5 (GE Healthcare) anti-mouse secondary antibody was used. The FIJI software was used to determine and analyse densitometric profiles.

### 4.6. BN-PAGE analyses

For BN-PAGE, 50 μg of crude heart mitochondria and 150 μg of crude liver mitochondria proteins were incubated with digitonin extraction buffer (HEPES (30 mM), potassium Acetate (150 mM), Glycerol (12%), 6-Aminocaproic acid (2 mM), EDTA (2 mM), high-purity digitonin (3 g/g), pH 7.2), and vortexed 1 h at 4 °C to solubilize membranes. After incubation, mitochondria were centrifugated at 30,000*g* for 20 min, supernatants were collected and mixed with loading dye (0.0125% (w/v), Coomassie brilliant blue G-250). Native complexes were resolved using Bis-Tris Invitrogen™ Novex™ NativePAGE™ 3–12% or 4–16% acrylamide gradient. To reach the optimal separation and resolution of OXPHOS supramolecular organisations, digitonine solubilized proteins were loaded on 3–12% gradient gel and were migrated at 10 mA for 12 h at 4 °C (complex II are not retained in the gel after overnight run). To analyse the complex II assembly, 4–16% gradient gels were migrated 6 h in order to keep the complex II in gel and for optimal separation of RC supercomplexes. RC complexes were detected using in-gel activity (IGA) assays as described previously [70]. Briefly, native gels were washed and incubated in a potassium phosphate buffer (50 mM, pH 7.2) containing iodonitrotetrazolium (1 mg/ml) supplemented with NADH (400 μM, pH 7.2) for complex I or Succinate (50 mM, pH 7.2) and Phenazine Methosulfate (20 mM) for complex II. For complex IV in-gel activity assays, native gels were incubated in RB containing Diaminobenzidine (1 mg/ml) and cytochrome *c* (0.5 mg/ml). Coomassie staining was performed with PageBlue protein staining solution. Colorimetric bands were recorded with Optical Densitometry of an Amersham ImageQuant 800.

Proteins were also immunodetected, gels were incubated in Towbin buffer (Tris (0.3% w/v), Glycine (1.44% w/v), Ethanol (10% *v*/v)) supplemented with SDS (0.2% v/v) and β-mercaptoethanol (0.2% v/v) for 30 min at RT, to denature proteins. Then gels were transferred on polyvinylidene difluoride (PVDF) in Towbin transfer buffer for 2 h at 0.2 A. Immunodetection was performed as described previously using the following primary antibodies: Anti-NDi1 (ref abcam: ab181848), anti-SDHC (ref protein tech: 14575-1-AP), anti-UQCRC2 (ref protein tech: 14742-1-AP), anti-COX1 ( ref thermofisher: #459600), peroxidase-

conjugated anti-mouse and anti-rabbit IgGs and Amersham CyDye 800 goat anti-rabbit and anti-mouse were used for immunodetection by chemiluminescence and fluorescence. Immunoreactive bands were recorded with an Amersham ImageQuant 800.

BN-PAGE gels after first dimension electrophoresis, were ran in a denaturing second dimension electrophoresis (2D-SDS PAGE). After collecting the first-dimension band and before the second dimension, first dimension bands were incubated in an Invitrogen™ Bolt™ MOPS SDS Running Buffer (Fisher Scientific) supplemented with β-mercaptoethanol (1% v/v) for 30 min at RT. Acrylamide gradient Bolt™ 4–12% Bis-Tris Plus Gels (Thermo Scientific) were used for 2D SDS-PAGE, the gels were transferred and immunodetection was performed as previously described for classical SDS-PAGE. Immunoreactive bands were incubated with primary antibody (coktil OXPHOS: ab110413) and detected recording fluorescence and chemiluminescence with an Amersham ImageQuant 800. The FIJI software was used to quantify the perform densitometry analyses of images obtained.

### 4.7. Oxaloacetate quantification

Oxaloacetate level was measured using enzymatic assay based on citrate synthase activity. Intact heart (200 μg) and liver (1000 μg) mitochondria were incubated like for oxygen consumption measurement in an Oxygraph-2 k at 37 °C. Briefly, 150 μl of mitochondria incubated in 2.1 ml RB consuming oxygen under uncoupled condition were collected and quenched with 50 μl ice cold acidic perchloric acid (PCA 7% without EDTA) every 30 s for three sampling during steady state uncoupled respiration, to assess steady state level of oxaloacetate. Samples were then centrifuged 10 min at 30,000*g* and supernatants were quickly neutralized with KOMO (KOH (2 M); MOPS (0.5 M)). OAA content was then quantified using citrate synthase buffer (Acetyl-CoA (200 μM)), 5,5′-dithiobis-(2-nitrobenzoic acid) (200 μM), Citrate Synthase from pig heart (4 U/ml) in phosphate buffer (50 mM, pH 7.2). Absorbance was recorded at 412 nm in UV Greiner bio-one 96-well plate by a CLARIOstar plate reader (BMG Labtech). Standard curve allowing OAA quantification was determined using fresh OAA solution.

### 4.8. NADH oxidation flux measurement ($JNAD^+$)

$NAD^+$ production rate was measured using enzymatic assay using G6PDH from *Leuconostoc mesenteroides*. Permeabilized mitochondria from heart (50 μg) and liver (100 μg) were incubated in 2.1 ml of potassium phosphate buffer (50 mM) with saturating concentrations of cytochrome *c* (62.5 μg/ml), NADH (0.625 mM) and succinate (10 mM) in an Oxygraph-2k at 37 °C. Five sampling of 150 μl of mitochondria incubated in potassium phosphate buffer (50 mM) were collected and quenched with 50 μl ice cold acidic perchloric acid (PCA 7% without EDTA) every 2.5 min. Samples were then centrifuged 10 min at 30,000*g* and supernatants were quickly neutralized with KOMO (KOH (2 M); MOPS (0.5 M)). Neutralized samples were then subjected to enzymatic assay quantifying $NAD^+$ content as described previously [50].

### 4.9. Mitochondrial NAD(P)H quantification

NADH level was measured in intact mitochondria, using respectively 100 μg/ml of heart mitochondria and 250 μg/ml of liver mitochondria, by fluorescence (λexc 340 nm; λem: 460 nm) at 37 °C, under agitation with an FP-8500 Spectrofluorometer (Jasko). Intact mitochondria from heart and liver were diluted in MIB + BSA and incubated with the different substrates conditions in an High Precision Cell quartz glass (10x10mm; HellmaAnalytics).

### 4.10. Fumarate and Malate metabolic flux measurement

Metabolic fluxes were measured by $^1$H—1D NMR. Intact Heart mitochondria were incubated in the same conditions than oxygen consumption measurements in an Oxygraph-2 k at 37 °C. During steady state respiration assessed under uncoupled conditions, aliquots collected at 0, 5, 7.5, and 12.5 min of incubation were snap frozen in liquid nitrogen to quench biochemical reactions. Metabolites were extracted with a mix of acetonitrile (ACN) and methanol (MeOH) to a final ACN/MeOH/Water proportion of 2:2:1. They were then vortexed, incubated at −20C for 20 min, and evaporated with a ThermoFisher SpeedVac SC250EXP concentrator. Samples were then dissolved into 200 μL $D_2O$ solution containing 2 mM Trimethyl-sillyl-propionic acid $d_4$ (TSPd4) used as NMR reference standard, and centrifuged to remove membrane debris. A final 180 μL volume of the resulting supernatants were transferred into 3 mm NMR tubes. Samples were analyzed by 1H—1D NMR on a Bruker Ascend 800 MHz NMR spectrometer equipped with a 5 mm QPCI cryoprobe. A quantitative zgpr30 sequence was used with 64 k acquisition points during 128 scans. The total repetition time between scans was set to 7 s. Malate and fumarate concentrations were quantified from their respective signals in the 1H—1D NMR spectra using TSPd4 as internal standard. All measurements were performed in triplicates.

### 4.11. Statistical analyses

Data are presented as mean ± SEM unless otherwise indicated in figure legends. Sample number (n) indicates the number of independent biological samples (individual mice) for each experiment. Sample numbers and experimental repeats are indicated in the figures. Data were analyzed with the GraphPad Prism software using unpaired Student's *t*-test, one-way ANOVA using Turkey's multiple comparison test, or two-way ANOVA using Bonferroni multiple comparison test between group comparison, as appropriate. A 0.05 *p*-value was considered statistically significant.

## Declaration of competing interest

Authors declare no conflict of interest.

## Acknowledgements

We gratefully acknowledge for the support, encouragement and useful discussions provided by Dr. Manuel Rojo. We would like to thank Prof. Michel Rigoulet and Prof. Nils-Göran Larsson, Dr. Dusanka Milenkovic for their precious feedback on the manuscript. We also thank Benoit Rousseau and Julien Izotte for the work at animal house (the service commun des animaleries, Animalerie A2 – University of Bordeaux). This work was supported by the AFM-Telethon Trampoline (AFM-19613), INCa-Cancéropôle GSO (N°2020-EM27) and ANR (ANR-16-CE14-0013). The funders had no role in study design, data collection and analysis, decision to publish, or preparation of the manuscript. MetaboHub-MetaToul (Metabolomics & Fluxomics facilities, Toulouse, France, http://www.metatoul.fr) is supported by the ANR grant MetaboHUB-ANR-11-INBS-0010. JCP is grateful to INSERM for funding a temporary full-time researcher position.

## Appendix A. Supplementary data

Supplementary data to this article can be found online at https://doi.org/10.1016/j.bbabio.2022.148532.

## References

[1] P. Mitchell, Coupling of phosphorylation to electron and hydrogen transfer by a chemi-osmotic type of mechanism, Nature 191 (1961) 144–148, https://doi.org/10.1038/191144a0.

[2] H.F. Alkan, P.W. Vesely, H. Hackl, J. Foßelteder, D.R. Schmidt, M.G. Vander Heiden, M. Pichler, G. Hoefler, J.G. Bogner-Strauss, Deficiency of malate-aspartate shuttle component SLC25A12 induces pulmonary metastasis, Cancer Metab. 8 (2020) 26, https://doi.org/10.1186/s40170-020-00232-7.

[3] P. Borst, The malate–aspartate shuttle (Borst cycle): how it started and developed into a major metabolic pathway, IUBMB Life 72 (2020) 2241–2259, https://doi.org/10.1002/iub.2367.

[4] W.-C. Lee, X. Ji, I. Nissim, F. Long, Malic enzyme couples mitochondria with aerobic glycolysis in osteoblasts, Cell Rep. 32 (2020), 108108, https://doi.org/10.1016/j.celrep.2020.108108.

[5] A.I. Cederbaum, C.S. Lieber, D.S. Beattie, E. Rubin, Characterization of shuttle mechanisms for the transport of reducing equivalents into mitochondria, Arch. Biochem. Biophys. 158 (1973) 763–781, https://doi.org/10.1016/0003-9861(73)90571-7.

[6] A.G. Dawson, Oxidation of cytosolic NADH formed during aerobic metabolism in mammalian cells, Trends Biochem. Sci. 4 (1979) 171–176, https://doi.org/10.1016/0968-0004(79)90417-1.

[7] B. Safer, C.M. Smith, J.R. Williamson, Control of the transport of reducing equivalents across the mitochondrial membrane in perfused rat heart, J. Mol. Cell. Cardiol. 2 (1971) 111–124, https://doi.org/10.1016/0022-2828(71)90065-4.

[8] K.F. LaNoue, A.J. Meijer, A. Brouwer, Evidence for electrogenic aspartate transport in rat liver mitochondria, Arch. Biochem. Biophys. 161 (1974) 544–550, https://doi.org/10.1016/0003-9861(74)90337-3.

[9] K.F. LaNoue, E.I. Wałajtys, J.R. Williamson, Regulation of glutamate metabolism and interactions with the citric acid cycle in rat heart mitochondria, J. Biol. Chem. 248 (1973) 7171–7183.

[10] B.E. Baysal, R.E. Ferrell, J.E. Willett-Brozick, E.C. Lawrence, D. Myssiorek, A. Bosch, A. van der Mey, P.E. Taschner, W.S. Rubinstein, E.N. Myers, C. W. Richard, C.J. Cornelisse, P. Devilee, B. Devlin, Mutations in SDHD, a mitochondrial complex II gene, in hereditary paraganglioma, Science 287 (2000) 848–851, https://doi.org/10.1126/science.287.5454.848.

[11] S.E. Browne, A.C. Bowling, U. Macgarvey, M.J. Baik, S.C. Berger, M.M.K. Muquit, E.D. Bird, M.F. Beal, Oxidative damage and metabolic dysfunction in Huntington's disease: selective vulnerability of the basal ganglia, Ann. Neurol. 41 (1997) 646–653, https://doi.org/10.1002/ana.410410514.

[12] E.T. Chouchani, V.R. Pell, E. Gaude, D. Aksentijević, S.Y. Sundier, E.L. Robb, A. Logan, S.M. Nadtochiy, E.N.J. Ord, A.C. Smith, F. Eyassu, R. Shirley, C.-H. Hu, A.J. Dare, A.M. James, S. Rogatti, R.C. Hartley, S. Eaton, A.S.H. Costa, P. S. Brookes, S.M. Davidson, M.R. Duchen, K. Saeb-Parsy, M.J. Shattock, A. J. Robinson, L.M. Work, C. Frezza, T. Krieg, M.P. Murphy, Ischaemic accumulation of succinate controls reperfusion injury through mitochondrial ROS, Nature 515 (2014) 431–435, https://doi.org/10.1038/nature13909.

[13] S. Dröse, Differential effects of complex II on mitochondrial ROS production and their relation to cardioprotective pre- and postconditioning, Biochim. Biophys. Acta 1827 (2013) 578–587, https://doi.org/10.1016/j.bbabio.2013.01.004.

[14] J. Zhang, Y.T. Wang, J.H. Miller, M.M. Day, J.C. Munger, P.S. Brookes, Accumulation of succinate in cardiac ischemia primarily occurs via canonical Krebs cycle activity, Cell Rep. 23 (2018) 2617–2628, https://doi.org/10.1016/j.celrep.2018.04.104.

[15] E.L. Mills, B. Kelly, A. Logan, A.S.H. Costa, M. Varma, C.E. Bryant, P. Tourlomousis, J.H.M. Däbritz, E. Gottlieb, I. Latorre, S.C. Corr, G. McManus, D. Ryan, H.T. Jacobs, M. Szibor, R.J. Xavier, T. Braun, C. Frezza, M.P. Murphy, L.A. O'Neill, Succinate dehydrogenase supports metabolic repurposing of mitochondria to drive inflammatory macrophages, Cell 167 (2016) 457–470, https://doi.org/10.1016/j.cell.2016.08.064, e13.

[16] J. Favier, L. Amar, A.-P. Gimenez-Roqueplo, Paraganglioma and phaeochromocytoma: from genetics to personalized medicine, Nat. Rev. Endocrinol. 11 (2015) 101–111, https://doi.org/10.1038/nrendo.2014.188.

[17] A. King, M.A. Selak, E. Gottlieb, Succinate dehydrogenase and fumarate hydratase: linking mitochondrial dysfunction and cancer, Oncogene 25 (2006) 4675–4682, https://doi.org/10.1038/sj.onc.1209594.

[18] M.A. Selak, S.M. Armour, E.D. MacKenzie, H. Boulahbel, D.G. Watson, K. D. Mansfield, Y. Pan, M.C. Simon, C.B. Thompson, E. Gottlieb, Succinate links TCA cycle dysfunction to oncogenesis by inhibiting HIF-alpha prolyl hydroxylase, Cancer Cell 7 (2005) 77–85, https://doi.org/10.1016/j.ccr.2004.11.022.

[19] L.W.S. Finley, W. Haas, V. Desquiret-Dumas, D.C. Wallace, V. Procaccio, S.P. Gygi, M.C. Haigis, Succinate dehydrogenase is a direct target of sirtuin 3 deacetylase activity, PLoS One 6 (2011), e23295, https://doi.org/10.1371/journal.pone.0023295.

[20] W. He, F.J.-P. Miao, D.C.-H. Lin, R.T. Schwandner, Z. Wang, J. Gao, J.-L. Chen, H. Tlan, L. Ling, Citric acid cycle intermediates as ligands for orphan G-protein-coupled receptors, Nature 429 (2004) 188–193, https://doi.org/10.1038/nature02488.

[21] Z. Zhang, M. Tan, Z. Xie, L. Dai, Y. Chen, Y. Zhao, Identification of lysine succinylation as a new post-translational modification, Nat. Chem. Biol. 7 (2011) 58–63, https://doi.org/10.1038/nchembio.495.

[22] H. Schägger, K. Pfeiffer, Supercomplexes in the respiratory chains of yeast and mammalian mitochondria, EMBO J. 19 (2000) 1777–1783, https://doi.org/10.1093/emboj/19.8.1777.

[23] R. Acín-Pérez, P. Fernández-Silva, M.L. Peleato, A. Pérez-Martos, J.A. Enriquez, Respiratory active mitochondrial supercomplexes, Mol. Cell 32 (2008) 529–539, https://doi.org/10.1016/j.molcel.2008.10.021.

[24] N.V. Dudkina, R. Kouřil, K. Peters, H.-P. Braun, E.J. Boekema, Structure and function of mitochondrial supercomplexes, Biochim. Biophys. Acta Bioenerg. 1797 (2010) 664–670, https://doi.org/10.1016/j.bbabio.2009.12.013, 16th European Bioenergetics Conference 2010.

[25] J.D. Chavez, C.F. Lee, A. Caudal, A. Keller, R. Tian, J.E. Bruce, Chemical crosslinking mass spectrometry analysis of protein conformations and supercomplexes in heart tissue, Cell Syst. 6 (2018) 136–141.e5, https://doi.org/10.1016/j.cels.2017.10.017.

[26] K.M. Davies, T.B. Blum, W. Kühlbrandt, Conserved in situ arrangement of complex I and III2 in mitochondrial respiratory chain supercomplexes of mammals, yeast, and plants, Proc. Natl. Acad. Sci. U. S. A. 115 (2018) 3024–3029, https://doi.org/10.1073/pnas.1720702115.

[27] J. Gu, M. Wu, R. Guo, K. Yan, J. Lei, N. Gao, M. Yang, The architecture of the mammalian respirasome, Nature 537 (2016) 639–643, https://doi.org/10.1038/nature19359.

[28] J.A. Letts, K. Fiedorczuk, L.A. Sazanov, The architecture of respiratory supercomplexes, Nature 537 (2016) 644–648, https://doi.org/10.1038/nature19774.

[29] B. Rieger, D.N. Shalaeva, A.-C. Söhnel, W. Kohl, P. Duwe, A.Y. Mulkidjanian, K. B. Busch, Lifetime imaging of GFP at CoxVIIIa reports respiratory supercomplex assembly in live cells, Sci. Rep. 7 (2017) 46055, https://doi.org/10.1038/srep46055.

[30] E. Balsa, M.S. Soustek, A. Thomas, S. Cogliati, C. García-Poyatos, E. Martín-García, M. Jedrychowski, S.P. Gygi, J.A. Enriquez, P. Puigserver, ER and nutrient stress promote assembly of respiratory chain supercomplexes through the PERK-eIF2α Axis, Mol. Cell 74 (2019) 877–890, https://doi.org/10.1016/j.molcel.2019.03.031, e6.

[31] C. Bianchi, M.L. Genova, G. Parenti Castelli, G. Lenaz, The mitochondrial respiratory chain is partially organized in a supercomplex assembly: kinetic evidence using flux control analysis, J. Biol. Chem. 279 (2004) 36562–36569, https://doi.org/10.1074/jbc.M405135200.

[32] E. Lapuente-Brun, R. Moreno-Loshuertos, R. Acín-Pérez, A. Latorre-Pellicer, C. Colás, E. Balsa, E. Perales-Clemente, P.M. Quirós, E. Calvo, M.A. Rodríguez-Hernández, P. Navas, R. Cruz, Á. Carracedo, C. López-Otín, A. Pérez-Martos, P. Fernández-Silva, E. Fernández-Vizarra, J.A. Enríquez, Supercomplex assembly determines electron flux in the mitochondrial electron transport chain, Science 340 (2013) 1567–1570, https://doi.org/10.1126/science.1230381.

[33] J.N. Blaza, R. Serreli, A.J.Y. Jones, K. Mohammed, J. Hirst, Kinetic evidence against partitioning of the ubiquinone pool and the catalytic relevance of respiratory-chain supercomplexes, Proc. Natl. Acad. Sci. U. S. A. 111 (2014) 15735–15740, https://doi.org/10.1073/pnas.1413855111.

[34] J.G. Fedor, J. Hirst, Mitochondrial supercomplexes do not enhance catalysis by quinone channeling, Cell Metab. 28 (2018) 525–531, https://doi.org/10.1016/j.cmet.2018.05.024, e4.

[35] M. Trouillard, B. Meunier, F. Rappaport, Questioning the functional relevance of mitochondrial supercomplexes by time-resolved analysis of the respiratory chain, Proc. Natl. Acad. Sci. 108 (2011) E1027–E1034, https://doi.org/10.1073/pnas.1109510108.

[36] A.B. Oestreicher, S.G. Van den Bergh, E.C. Slater, The inhibition by 2,4-dinitrophenol of the removal of oxaloacetate formed by the oxidation of succinate by rat-liver and -heart mitochondria, Biochim. Biophys. Acta, Bioenerg. 180 (1969) 45–55, https://doi.org/10.1016/0005-2728(69)90192-3.

[37] P. Schollmeyer, M. Klingenberg, Oxaloacetate and adenosinetriphosphate levels during inhibition and activation of succinate oxidation, Biochem. Biophys. Res. Commun. 4 (1961) 43–47, https://doi.org/10.1016/0006-291x(61)90252-2.

[38] L. Wojtczak, A.B. Wojtczak, L. Ernster, The inhibition of succinate dehydrogenase by oxaloacetate, Biochim. Biophys. Acta, Enzymol. 191 (1969) 10–21, https://doi.org/10.1016/0005-2744(69)90310-6.

[39] W.P. Zeylemaker, A.D.M. Klaasse, E.C. Slater, Studies on succinate dehydrogenase: V. Inhibition by oxaloacetate, Biochim. Biophys. Acta, Enzymol. 191 (1969) 229–238, https://doi.org/10.1016/0005-2744(69)90242-3.

[40] B.D. Fink, F. Bai, L. Yu, R.D. Sheldon, A. Sharma, E.B. Taylor, W.I. Sivitz, Oxaloacetic acid mediates ADP-dependent inhibition of mitochondrial complex II-driven respiration, J. Biol. Chem. 293 (2018) 19932–19941, https://doi.org/10.1074/jbc.RA118.005144.

[41] B.D. Fink, L. Yu, W.I. Sivitz, Modulation of complex II-energized respiration in muscle, heart, and brown adipose mitochondria by oxaloacetate and complex I electron flow, FASEB J. 33 (2019) 11696–11705, https://doi.org/10.1096/fj.201900690R.

[42] B. Safer, The metabolic significance of the malate-aspartate cycle in heart, Circ. Res. 37 (1975) 527–533, https://doi.org/10.1161/01.RES.37.5.527.

[43] T. Brandt, A. Mourier, L.S. Tain, L. Partridge, N.-G. Larsson, W. Kühlbrandt, Changes of mitochondrial ultrastructure and function during ageing in mice and Drosophila, elife 6 (2017), e24662, https://doi.org/10.7554/eLife.24662.

[44] J.A. Enríquez, Supramolecular organization of respiratory complexes, Annu. Rev. Physiol. 78 (2016) 533–561, https://doi.org/10.1146/annurev-physiol-021115-105031.

[45] C. Greggio, P. Jha, S.S. Kulkarni, S. Lagarrigue, N.T. Broskey, M. Boutant, X. Wang, S. Conde Alonso, E. Ofori, J. Auwerx, C. Cantó, F. Amati, Enhanced respiratory chain supercomplex formation in response to exercise in human skeletal muscle, Cell Metab. 25 (2017) 301–311, https://doi.org/10.1016/j.cmet.2016.11.004.

[46] H. Schägger, K. Pfeiffer, The ratio of oxidative phosphorylation complexes I-V in bovine heart mitochondria and the composition of respiratory chain Supercomplexes*, J. Biol. Chem. 276 (2001) 37861–37867, https://doi.org/10.1074/jbc.M106474200.

[47] E. Gnaiger, Capacity of oxidative phosphorylation in human skeletal muscle: new perspectives of mitochondrial physiology, Int. J. Biochem. Cell Biol. 41 (2009) 1837–1845, https://doi.org/10.1016/j.biocel.2009.03.013.

[48] J.J. Hautecler, C.M. Sluse-Goffart, A. Evens, C. Duyckaerts, F.E. Sluse, Effect of aspartate and glutamate on the oxoglutarate carrier investigated in rat heart mitochondria and inverted submitochondrial vesicles, Biochim. Biophys. Acta, Bioenerg. 1185 (1994) 153–159, https://doi.org/10.1016/0005-2728(94)90205-4.

[49] E.A. Siess, D.G. Brocks, O.H. Wieland, in: Distribution of Metabolites Between the Cytosolic and Mitochondrial Compartments of Hepatocytes Isolated From Fed Rats 359, 1978, pp. 785–798, https://doi.org/10.1515/bchm2.1978.359.2.785.
[50] O. Bunoust, A. Devin, N. Avéret, N. Camougrand, M. Rigoulet, Competition of electrons to enter the respiratory chain: a new regulatory mechanism of oxidative metabolism in saccharomyces cerevisiae, J. Biol. Chem. 280 (2005) 3407–3413, https://doi.org/10.1074/jbc.M407746200.
[51] A. Mourier, A. Devin, M. Rigoulet, Active proton leak in mitochondria: a new way to regulate substrate oxidation, Biochim. Biophys. Acta 1797 (2010) 255–261, https://doi.org/10.1016/j.bbabio.2009.10.011.
[52] I.-L. Påhlman, L. Gustafsson, M. Rigoulet, C. Larsson, Cytosolic redox metabolism in aerobic chemostat cultures of Saccharomyces cerevisiae, Yeast 18 (2001) 611–620, https://doi.org/10.1002/yea.709.
[53] M. Rigoulet, A. Mourier, A. Galinier, L. Casteilla, A. Devin, Electron competition process in respiratory chain: regulatory mechanisms and physiological functions, Biochim. Biophys. Acta 1797 (2010) 671–677, https://doi.org/10.1016/j.bbabio.2010.01.030.
[54] P. Carneiro, M. Duarte, A. Videira, The main external alternative NAD(P)H dehydrogenase of neurospora crassa mitochondria, Biochim. Biophys. Acta 1608 (2004) 45–52, https://doi.org/10.1016/j.bbabio.2003.10.004.
[55] S. Foriel, G.H. Renkema, Y. Lasarzewski, J. Berkhout, R.J. Rodenburg, J.A. M. Smeitink, J. Beyrath, A. Schenck, A drosophila mitochondrial complex I deficiency phenotype array, Front. Genet. 10 (2019), https://doi.org/10.3389/fgene.2019.00245.
[56] L.I. Grad, B.D. Lemire, Mitochondrial complex I mutations in Caenorhabditis elegans produce cytochrome c oxidase deficiency, oxidative stress and vitamin-responsive lactic acidosis, Hum. Mol. Genet. 13 (2004) 303–314, https://doi.org/10.1093/hmg/ddh027.
[57] M.A.H. Luttik, K.M. Overkamp, P. Kötter, S. de Vries, J.P. van Dijken, J.T. Pronk, The Saccharomyces cerevisiae NDE1 and NDE2 genes encode separate mitochondrial NADH dehydrogenases catalyzing the oxidation of cytosolic NADH *, J. Biol. Chem. 273 (1998) 24529–24534, https://doi.org/10.1074/jbc.273.38.24529.
[58] S. Ait-El-Mkadem, M. Dayem-Quere, M. Gusic, A. Chaussenot, S. Bannwarth, B. François, E.C. Genin, K. Fragaki, C.L.M. Volker-Touw, C. Vasnier, V. Serre, F. Lespinasse, S. Richter, G. Eisenhofer, C. Rouzier, F. Mochel, A. De Saint-Martin, M.-T. Abi Warde, Jans JJM, J. Amiel, Z. Avsec, C. Mertes, T.B. Haack, T. Strom, T. Meitinger, P.E. Bonnen, R.W. Taylor, J. Gagneur, P.M. van Hasselt, A. Rötig, A. Delahodde, H. Prokisch, S.A. Fuchs, V. Paquis-Flucklinger, M.G.M. de Sain-van der Velde, K.L.I. van Gassen, Mutations in MDH2, encoding a Krebs cycle enzyme, cause early-onset severe encephalopathy, Am. J. Hum. Genet. 100 (2017) 151–159, https://doi.org/10.1016/j.ajhg.2016.11.014.
[59] D.J. Hayes, D.J. Taylor, P.J. Bore, D. Hilton-Jones, D.L. Arnold, M.V. Squier, A. E. Gent, G.K. Radda, An unusual metabolic myopathy: a malate-aspartate shuttle defect, J. Neurol. Sci. 82 (1987) 27–39, https://doi.org/10.1016/0022-510x(87)90004-9.
[60] A. Munnich, P. Rustin, Clinical spectrum and diagnosis of mitochondrial disorders, Am. J. Med. Genet. 106 (2001) 4–17, https://doi.org/10.1002/ajmg.1391.
[61] C.D.M. van Karnebeek, R.J. Ramos, X.-Y. Wen, M. Tarailo-Graovac, J.G. Gleeson, C. Skrypnyk, K. Brand-Arzamendi, F. Karbassi, M.Y. Issa, R. van der Lee, B. I. Drögemöller, J. Koster, J. Rousseau, P.M. Campeau, Y. Wang, F. Cao, M. Li, J. Ruiter, J. Ciapaite, L.A.J. Kluijtmans, M.A.A.P. Willemsen, J.J. Jans, C.J. Ross, L. T. Wintjes, R.J. Rodenburg, M.C.D.G. Huigen, Z. Jia, H.R. Waterham, W. W. Wasserman, R.J.A. Wanders, N.M. Verhoeven-Duif, M.S. Zaki, R.A. Wevers, Bi-allelic GOT2 mutations cause a treatable malate-aspartate shuttle-related encephalopathy, Am. J. Hum. Genet. 105 (2019) 534–548, https://doi.org/10.1016/j.ajhg.2019.07.015.
[62] K. Birsoy, T. Wang, W.W. Chen, E. Freinkman, M. Abu-Remaileh, D.M. Sabatini, An essential role of the mitochondrial electron transport chain in cell proliferation is to enable aspartate synthesis, Cell 162 (2015) 540–551, https://doi.org/10.1016/j.cell.2015.07.016.
[63] L.B. Sullivan, D.Y. Gui, A.M. Hosios, L.N. Bush, E. Freinkman, M.G. Vander Heiden, Supporting aspartate biosynthesis is an essential function of respiration in proliferating cells, Cell 162 (2015) 552–563, https://doi.org/10.1016/j.cell.2015.07.017.
[64] J.L. Purvis, J.M. Lowenstein, The relation between intra- and extramitochondrial pyridine nucleotides, J. Biol. Chem. 236 (1961) 2794–2803, https://doi.org/10.1016/S0021-9258(19)61739-4.
[65] A. Davila, L. Liu, K. Chellappa, P. Redpath, E. Nakamaru-Ogiso, L.M. Paolella, Z. Zhang, M.E. Migaud, J.D. Rabinowitz, J.A. Baur, Nicotinamide adenine dinucleotide is transported into mammalian mitochondria, elife 7 (2018), e33246, https://doi.org/10.7554/eLife.33246.
[66] T.S. Luongo, J.M. Eller, M.-J. Lu, M. Niere, F. Raith, C. Perry, M.R. Bornstein, P. Oliphint, L. Wang, M.R. McReynolds, M.E. Migaud, J.D. Rabinowitz, F. B. Johnson, K. Johnsson, M. Ziegler, X.A. Cambronne, J.A. Baur, SLC25A51 is a mammalian mitochondrial NAD+ transporter, Nature 588 (2020) 174–179, https://doi.org/10.1038/s41586-020-2741-7.
[67] A. Mourier, E. Motori, T. Brandt, M. Lagouge, I. Atanassov, A. Galinier, G. Rappl, S. Brodesser, K. Hultenby, C. Dieterich, N.-G. Larsson, Mitofusin 2 is required to maintain mitochondrial coenzyme Q levels, J. Cell Biol. 208 (2015) 429–442, https://doi.org/10.1083/jcb.201411100.
[68] A. Mourier, S. Matic, B. Ruzzenente, N.-G. Larsson, D. Milenkovic, The respiratory chain supercomplex organization is independent of COX7a2l isoforms, Cell Metab. 20 (2014) 1069–1075, https://doi.org/10.1016/j.cmet.2014.11.005.
[69] U.K. Laemmli, Cleavage of structural proteins during the assembly of the head of bacteriophage T4, Nature 227 (1970) 680–685, https://doi.org/10.1038/227680a0.
[70] Wittiget al., n.d., I Wittig R Carrozzo FM Santorelli H. Schägger n.d. Functional assays in high-resolution clear native gels to quantify mitochondrial complexes in human biopsies and cell lines. Electrophoresis 28:3811–3820. doi:10.1002/elps.200700367.